



# Proof of Concept: In-Situ Wear Differentiation of Simultaneously Wearing Counterparts

Felix Harden<sup>1</sup> · Birgit Schädel<sup>1</sup> · Marlon Siegel<sup>1,2</sup> · Roland Kral<sup>1</sup> · Rainer Adelung<sup>3</sup> · Olaf Jacobs<sup>1</sup>

Received: 17 May 2023 / Accepted: 3 July 2023 / Published online: 19 July 2023  
© The Author(s) 2023

## Abstract

Accurate assessment of the tribological system's wear behavior is crucial for optimization. Common tribological test stands rely on a single measurement information—usually the indentation depth of the complete tribological system. If both counterparts experience wear—like polymer–polymer combinations—a subsequent assessment of the tested specimens is needed to estimate the contributions of each partner for determining the wear volume, and thus the wear rate. In this work, we propose a novel approach how an in-situ wear measurement of both simultaneously wearing counterparts can be implemented and generally demonstrate the feasibility on a ball-on-prism tribometer. This is achieved by measuring the system's indentation depth while simultaneously scanning the ball's surface with a laser profile scanner, providing information for calculation of the ball's wear volume. While offering new possibilities for wear evaluation, challenges remain including radial runout of the measured specimen, testing in media and accumulation of large amounts of debris. Overall, this work presents an advancement in the evaluation of wear behavior, enabling better optimization of tribological systems with simultaneous wear. Refinements and adaptations to different setups can further enhance its utility.

**Keywords** Tribology · Polymer–polymer · Sliding wear · Tribometer · 3D-image

## 1 Introduction

Tribological systems containing polymers often offer significant cost benefits especially for systems with low to medium loading. Furthermore, a significant reduction of the system weight as well as the omission of external lubricants can be achieved. In many cases polymer-metal systems are used. These tribological polymer-metal combinations are well researched [1–10]. Therefore, they have broad industrial applications.

Not only due to the new possibilities and increasing importance of additive manufacturing technologies, polymer–polymer tribological systems gain increasing interest [8–13]. Even though tribological polymer–polymer systems are no novelty, less information is published on them so far. One of the reasons might be that analyzing tribological polymer–polymer combinations comes with some additional challenges compared to polymer-metal or polymer-ceramic systems. Previous publications by Schädel et al. [14] and Harden et al. [15] have pointed out that differentiating the amount of wear between the partners is up to now a major challenge, regardless of the test system.

---

✉ Felix Harden  
felix.harden@th-luebeck.de

Birgit Schädel  
birgit.schaedel@th-luebeck.de

Marlon Siegel  
siegel.marlon@googlemail.com

Roland Kral  
roland.kral@th-luebeck.de

Rainer Adelung  
ra@tf.uni-kiel.de

Olaf Jacobs  
olaf.jacobs@th-luebeck.de

<sup>1</sup> Department of Mechanical Engineering and Business Administration, Technische Hochschule Lübeck, Mönkhof Weg 239, 23562 Lübeck, Germany

<sup>2</sup> Present Address: Implantcast GmbH, Lüneburger Schanze 26, 21614 Buxtehude, Germany

<sup>3</sup> Faculty of Engineering Department of Material Science Functional Nanomaterials Chair Kaiserstraße 2, Christian-Albrechts-Universität zu Kiel, 24143 Kiel, Germany

A major limitation that nearly all tribometers have in common is that usually the information about the wear volume is acquired via the indentation depth including wear of both partners (system wear). In combination with further assumptions, commonly the contact geometry, the wear volume of the system can be determined. For polymer-metal and polymer-ceramic combinations it can be assumed that the wear of the metal or ceramic part, respectively, is neglectable. Therefore, wear only occurs at the polymer. With these assumptions the wear volume can be calculated from the indentation depth.

When testing polymer–polymer combinations, both counterparts might experience significant wear to a different extent. Therefore, the assumptions previously made for polymer-metal and polymer-ceramic combinations do not apply anymore. As a result, the indentation depth cannot be directly related to one partner. It rather needs to be distributed between both partners. Assuming that only one partner experiences wear, two limiting cases are possible. The limiting cases of ball-prism geometries are shown in Fig. 1. It can be seen that the projected wear surface (Fig. 1a) is the same regardless which partner experiences wear. If only the prism exhibits wear, the wear volume (Fig. 1b) evolves as two spherical caps. In contrast, if the ball exhibits the complete wear (Fig. 1c) the projected wear surface is circumferentially removed from the ball.

For both cases, the wear volume can be calculated using the indentation depth and the geometry. Due to the different geometries and overlap ratios for the ball and the prism, the wear volume for both limiting cases strongly differs for the same indentation depth. An example of this described in a previous work [15] is shown in Fig. 2: The wear volume was calculated from the indentation depth under the assumption that only the ball experiences wear (blue curve) and for the case that only the prism is worn (red curve). For identification of the true wear scenario the specimens need to be inspected after the wear test. In many cases however, the assumption that only one partner

**Fig. 1** Possible limiting cases of polymer–polymer combinations in ball-on-prism tribometer: **a** projected wear surface, **b** wear of prism only, **c** wear of ball only [15]

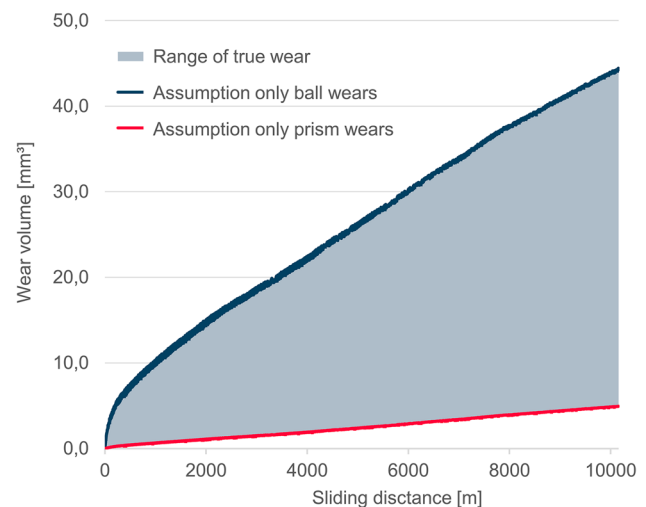
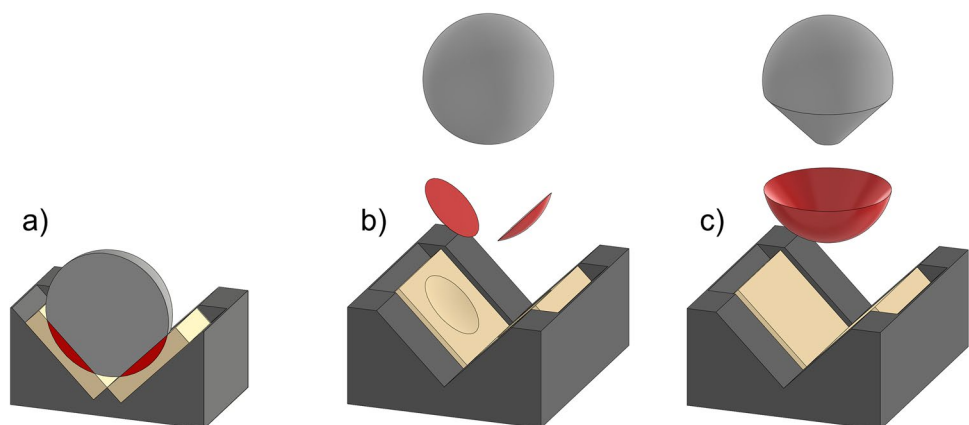


**Fig. 2** Comparison of the limiting cases calculated from the indentation depth of a wear test on a ball from tribologically optimized glycol modified polyethyleneterephthalate vs. a prism from acrylonitrile-styrene-acrylate-copolymer [15]

experiences wear is not accurate. The true wear volume of the system usually lies somewhere in between the limiting cases.

One possibility to increase accuracy in such cases is to measure the worn specimens after the test by topographical techniques. This method however, is very time consuming. Furthermore, it only shows the situation at the end of the test. An assumption that the percentual contributions of each partner stays constant throughout the whole experiment seems rather improbable. Pausing the test in between to generate additional topographical measurements comes with further problems. Many systems act sensitive to a restart. Often a restart is accompanied with another running in phase [16]. So far there have been different approaches to optimize the data acquisition of tribological test stands in order to get more detailed information about the wear, the evolving contact geometries and material properties.

Patent nr. CN101504357A [17] describes a tribometer similar to a pin-on-disk tribometer equipped with a surface topography instrument which is able to measure the topography of the lower specimen (disc) with a contactor. Up to a rotational speed of the lower specimen of 30 rpm the topography can be measured without stopping the test. Above 30 rpm the rotation needs to be stopped and continued after the measurement. The challenges concerning evaluation of simultaneous wear occurring on both partners cannot be solved with this setup since only the lower specimen is measured. Furthermore, measuring the topography with a contactor introduces a second tribological contact between the lower specimen and the contactor. This will influence the tribological behavior of the tested material combination.

An improved version of the tribometer is patented under patent nr. CN102607977B [18]. Here, the topographical measurement is done in a contact free manner by digital image processing of microscopic images. Nevertheless, the inventors also acknowledge that only the lower specimen can be inspected in-situ. A graphical inspection of the counter partner can be achieved by disassembly. The inventors of CN102607977B come to the same conclusion as described before. Disassembling one specimen for topographical analysis is time consuming and greatly limits the accuracy of the wear test if the specimen is reinstalled and the test is continued.

There are also other techniques to determine physical material information beyond topographical information. Patent nr. US10258239B2 [19] for example describes a tribometer setup that includes a Raman spectroscope. This allows much more detailed material investigation of the wear mark. However, this setup has the same issue as the previous inventions: the information can only be obtained at one partner. The second partner needs to be disassembled if it should be inspected.

Further approaches exist going in similar directions like for example US10024776B2 [20]. Despite all these approaches, if one wants to investigate the time dependent wear behavior of combinations where both partners experience significant wear—like in most polymer–polymer combinations—the problem of assigning the wear volume to the correct partner remains unsolved. The reason for that is that a second information related to the wear volume is

required. With current tribometers and their modifications usually only a single information related to the wear volume is measured.

## 2 Materials and Methods

During this work, a ball-on-prism tribometer was used. However, the method can be transferred to most common tribometers with at least one continuously moving specimen like for example pin-on-disc, ball-on-disc, block-on-ring or others with analog considerations.

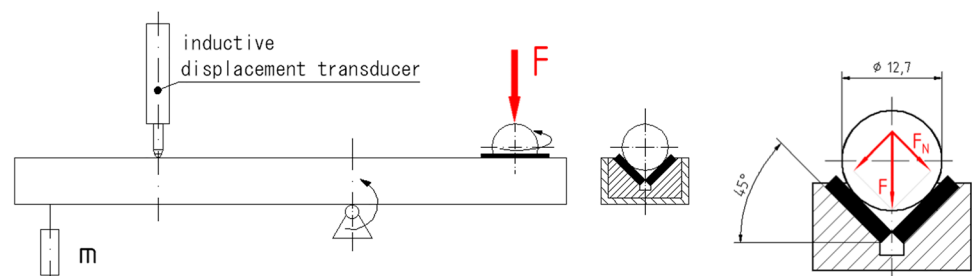
### 2.1 Tribological Test Stand

A ball-on-prism tribometer VPS6 from Dr. Tillwich GmbH Werner Stehr was used. Figure 3 shows a sketch of one of the six test sites of the VPS6. The prism contains two plates installed in an  $\pm 45^\circ$  angle to the vertical axis. It is installed on a lever which presses the prism against a ball by means of a dead weight at the other end of the lever. The force is defined by this dead weight and the leverage ratio. The ball is mounted in a special adapter and is driven by a speed-controlled motor. For digital data processing the test stand is equipped with inductive displacement transducers. They continuously measure the indentation depth over the whole experiment.

To be able to continuously differentiate the wear behavior of a polymer–polymer tribological system the above mentioned VPS6 was modified. For this proof of concept only one test site was used. However, details about expanding the modifications to the remaining five test sites will be addressed in Sect. 5.

As already described, the unmodified test stand measures the occurring wear via indentation depth. This information cannot be directly related to a single partner. In order to be able to differentiate the wear volume and assign it correctly to the partners, it is necessary to introduce a second measured information that can be directly related to the wear of a single partner. Furthermore, recording this measurement information should influence the tribological behavior as little as possible. This can be realized by optical topographical measurements. Therefore, the measured wear mark must be

**Fig. 3** Test principle of the ball-on-prism tribometer [15]



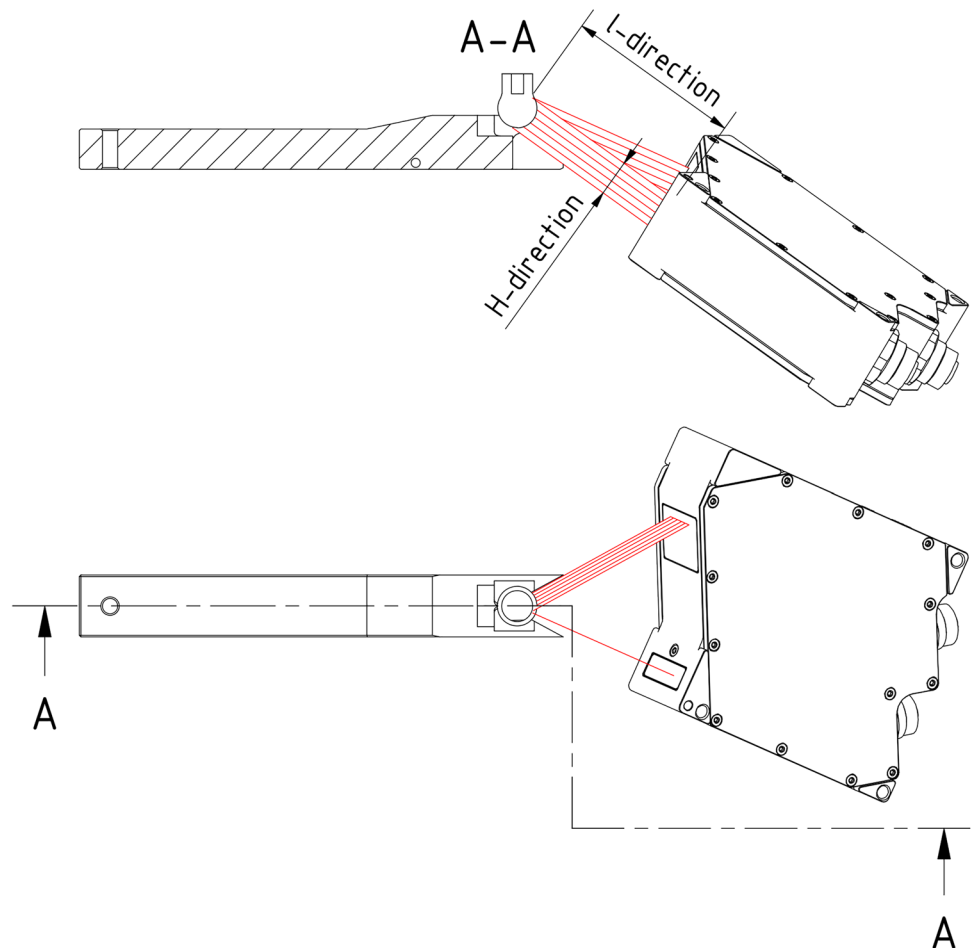
accessible. Measurements cannot be done on surfaces that are permanently in contact. In the case of the VPS6, the prisms are in a continuous contact while the rotating ball only has a partial contact on its circumferential surface. For this reason, a topographical measurement of the ball has been performed.

To gather the required topological information of the ball, a laser profile scanner scanCONTROL 2900 10/BL—abbrev. LPS—from Micro-Epsilon Messtechnik GmbH & Co. KG was used. It allows a simultaneous measurement of the depth from 1280 points arranged in a straight line resulting in a profile information. The system has a resolution of  $1\ \mu\text{m}$  in depth ( $l$ -direction) and a distance between the points ( $H$ -direction) of ca.  $8\ \mu\text{m}$ . Due to the design of the LPS, the distance between two measuring points might vary depending on the measured depth. Therefore, not only the  $l$ -direction is actively measured but also the  $H$ -position (zero position is in the center of the measuring field). Figure 4 shows the setup of the LPS installed on the tribometer in principle. The LPS is rigidly mounted on the VPS6. Since the wear mark on the ball will occur under  $45^\circ$ , the LPS is horizontally tilted by  $30^\circ$ . This enables to accurately measure nearly up to the tip of the ball. An alignment of the exiting beams with the

rotational axis of the ball was performed. For this purpose, a calibrating cylinder with a known diameter was installed instead of the ball and measured with the LPS. The LPS was shifted accordingly until the LPS was properly adjusted. In this position, the axis of rotation from the VPS6 was derived as a parallel line with an offset of the calibrating cylinder radius. The adjustment of the LPS needs to be done only once. In order to be able to project the laser beams onto the surface of the ball, a triangular opening is cut into the lever of the VPS6.

During this stage of the development, the data acquisition from the inductive displacement transducers as well as LPS was done separately and combined in a second step due to compatibility issues which shall be solved in future. The displacement transducer was connected to a measuring amplifier Spider8 from HBM (Hottinger Brüel & Kjaer GmbH) and the data were then recorded using the Software Catman Easy (Hottinger Brüel & Kjaer GmbH). After the test, the data set of indentation depth with according time stamp was exported as ASCII file. The data recording for the LPS was done using a LabVIEW Script supplied by Micro-Epsilon Messtechnik GmbH & Co. KG which was modified by the authors to suite the described application.

**Fig. 4** Schematic setup for measuring the balls wear in the VPS6



To minimize data volume and the area for possible artefacts, the recorded profile data were cut on both ends of the measurement width ( $H$ -direction) to the relevant portion for the wear test. In addition, functions for calibrating the rotational axis as well as defining the position of the prism relative to the ball were implemented. The measured values in  $H$ - and  $l$ -direction were saved to an ASCII-file. At the end of the test, the acquired data sets were used to calculate the wear volume and produce three-dimensional plots using a MATLAB scripts which can be found in the supplementary information.

To run friction and wear tests with this setup, no significant changes for the VPS6 are needed compared to the usual procedures. To improve the accuracy of the LSP, the system was started at least one hour before setting up the wear test. It allows the system to reach thermal equilibrium in the active state. A ball made of the desired material was installed in the designated mount of the VPS6. The prism was equipped with small platelets of the desired counterpart and installed in the lever. Both specimens, ball and prism, were cleaned with a suitable cleaning agent—in our case pure ethanol. By using the live data of the LPS, in a next step the position of the tip of the ball was determined as the intersection of the calibrated rotational axis and the contour of the ball. Furthermore, offset between the tip of the ball and the intersection of rotational axis and theoretical prism surface was determined. This is done by adapting the value until the line representing the prism is tangential to the plotted profile data. These values are later needed for the calculation of the wear volume. Afterwards the lever was installed in the VPS6 and the dead weight was put onto the lever resulting in normal force onto each plate of the prism of 21.21 N. Now the displacement transducers of the VPS6 are placed on the levers and adjusted to zero accordingly. After starting the rotation with 1 Hz rotational frequency, the data acquisition of the LPS and the inductive displacement transducers were started simultaneously. The data acquisition rate was 0.1 Hz over a test period of min. 24 h in standard atmosphere.

## 2.2 Materials and Validation Principle

For validation of this new measuring approach, different tribological combinations from a tribologically optimized glycol modified Polyethyleneterephthalate (PETG/PTFE), Polyamide 66 (PA66), Polylactic acid (PLA), Polyoxymethylene (POM), Acrylonitrile-styrene-acrylate (ASA), 100Cr6, and AlMg3, were used. The PETG/PTFE, PLA as well as the ASA specimens were produced via Fused Layer modeling, an additive manufacturing technique while the PA66 and the POM specimens were produced via injection molding.

Previous studies of polymer–polymer combinations like for example by Schädel et al. [14] and Harden et al. [15]

have shown several difficulties evaluating these combinations with post-wear measuring techniques, producing three-dimensional representations of the worn specimen. One issue is that the initial geometry of the specimen cannot be directly measured and must be assumed in order to evaluate the wear volume. Since the specimens are not perfect spheres or plates and exhibit imperfections, deviations from the true wear volume occur. Furthermore, attempting to evaluate the wear of the ball using a post-wear measuring technique requires precise determination of the ball's rotational axis or knowledge of the initial geometry in the exactly right position relative to the worn specimens. This task poses notable challenges with most post-wear measuring techniques often necessitating the use of mathematical fitting techniques introducing significant inaccuracies.

Due to these deviations between post-wear measurements and the newly developed measuring technique a comparison of the results does not provide strong evidence of validation not because of errors in the new measurement technic but primarily due to inaccuracy of post-wear measurement methods. Therefore, a systematic approach for validation was chosen, comparing our newly developed measuring technique with the well-established conventional technique always evaluating the same according indentation depth datasets.

The capability of measuring no wear at any partner needs to be proofed. Therefore, a ball form AlMg3 was installed in the test stand and measured over a period without running against any counterpart to proof the wear-free scenario.

The scenario of a wearing prism was validated by running an AlMg3 ball against a prism form PETG/PTFE. Since this combination ensures that only the prism experiences significant wear, a comparison was made between the results obtained from the newly developed measuring technique and the conventional technique.

A similar test is conducted to validate the scenario of a wearing ball. In this case, a ball from PA66 was tested against a prism form 100Cr6. This way it is certain that only the ball experiences significant wear. Again, a comparison of the results obtained with the new and the conventional technique was done.

The proof of concept is established after successfully demonstrating the ability to correctly evaluate both extreme cases, as well as the wear-free scenario. Additionally, various combinations of simultaneously wearing counterparts were tested to gain a more comprehensive understanding of the potentials and challenges of the new measuring technique.

All tested combinations with their according wear scenario are given in Table 1.

**Table 1** Material combinations

Nr	Ball	Prism	Wear scenario
1	AlMg3	None	Wear-free
2	AlMg3	PETG/PTFE	Wear of prism
3	PA66	100Cr6	Wear of ball
4	PETG/PTFE	PLA	Wear of both partners
5	POM	POM	Wear of both partners
6	ASA	ASA	Wear of both partners

### 3 Theory

#### 3.1 Calculations of Wear Volume

The setup described in the previous chapter and shown in Fig. 4 allows the direct calculation of the wear volume of the ball. In combination with the information about the indentation depth, the wear volume of the prism can be calculated. The

relevant dimensions and variables that are necessary for all calculations are given in Fig. 5.

The calculation is done incrementally. The shape of the ball at any time can be described by horizontal radii  $r_i(t)$  at different incremental heights  $h_i(t)$ .  $h_i(t)$  can be calculated using the measured data  $l_i(t)$  and  $H_i(t)$  from the LPS. Defining (1) and combining it with the geometrical relations shown in Fig. 5 and given by (2) to (5),  $h_i(t)$  can be described according to (6).

$$H_{i+1}(t) < H_i(t) \tag{1}$$

$$h_i(t) = c(t) - d(t) \tag{2}$$

$$c(t) = \frac{H_i(t) - H_{i+1}(t)}{\cos 30^\circ} \tag{3}$$

$$d(t) = \sin 30^\circ * [b(t) - \{l_{i+1}(t) - l_i(t)\}] \tag{4}$$

$$b(t) = \tan 30^\circ * \{H_i(t) - H_{i+1}(t)\} \tag{5}$$

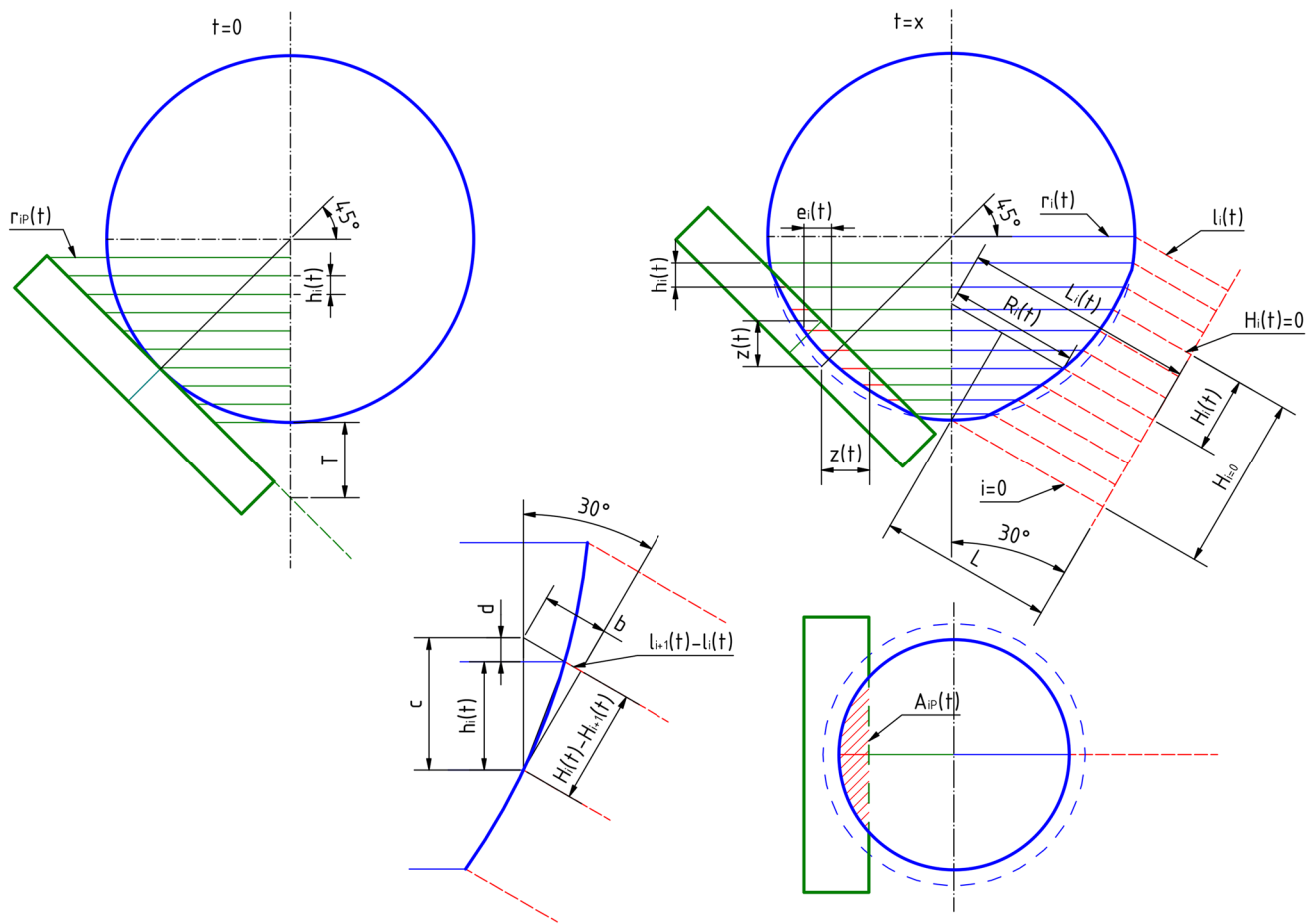


**Fig. 5** Sketch of relevant dimensions and variables for calculation of wear volume

$$h_i(t) = \frac{\sqrt{3}}{2} \{H_i(t) - H_{i+1}(t)\} + \frac{1}{2} \{l_{i+1}(t) - l_i(t)\} \quad (6)$$

Due to the initial calibration of the rotational axis and the known distance to the tip of the ball  $L$ , the theoretical distance to the rotational axis  $L_i(t)$  at every  $H_i(t)$  is known (7). With the measured data  $l_i(t)$  at every  $H_i(t)$ ,  $R_i(t)$  can be calculated (8). Considering the tilted angle of the LPS (9) leads to the formulation of  $r_i(t)$  (10).

$$L_i(t) = L + \tan 30^\circ * [H_{i=0} - H_i(t)] \quad (7)$$

$$R_i(t) = L_i(t) - l_i(t) \quad (8)$$

$$r_i(t) = R_i(t) * \cos 30^\circ \quad (9)$$

$$r_i(t) = \frac{\sqrt{3}}{2} \left\{ L + \frac{\sqrt{3}}{3} * [H_{i=0} - H_i(t)] - l_i(t) \right\} \quad (10)$$

The volume of the ball  $V_k(t)$ —within the measured area—can be approximated as shown in Formula (11). This is done by adding truncated cones with height  $h_i(t)$  (6) and different radii  $r_i(t)$  (10). The wear volume of the ball  $\Delta V_k(t)$  can be then calculated according to Formula (12).

$$V_k(t) = \frac{\pi}{3} \sum_i h_i(t) * [r_i(t)^2 + r_i(t) * r_{i+1}(t) + r_{i+1}(t)^2] \quad (11)$$

$$\Delta V_k(t) = V_k(t = 0) - V_k(t) \quad (12)$$

To be able to determine the wear volume of both plates of the prism  $\Delta V_p(t)$ , first the distance between the axis of rotation and the and the unworn surface of the prism  $r_{ip}(t)$  at every  $h_i(t)$  needs to be determined. First,  $r_{0p}(t)$  at the tip of the ball is determined. Due to the occurring wear and the angle of the prism,  $r_{0p}(t)$  is dependent on the indentation depth  $z(t)$  measured by the inductive displacement transducer. With the geometrical relations, the distance between the tip of the ball and the intersection of rotational axis and theoretical prism surface  $T$  at the beginning of the test  $r_{0p}(t)$  can be calculated according to Formula (13). Any other  $r_{ip}(t)$  can be then calculated using  $r_{0p}(t)$  and  $h_i(t)$  as shown in Formula (14). Inserting Formula (13) into Formula (14) leads to Formula (15).

$$r_{0p}(t) = T - z(t) \quad (13)$$

$$r_{ip}(t) = r_{0p}(t) + \sum_{i=0}^n h_i(t) \quad (14)$$

$$r_{ip}(t) = T - z(t) + \sum_{i=0}^n h_i(t) \quad (15)$$

With this information the horizontal indentation into the prisms  $e_i(t)$  can be calculated by Formula (16). For all  $e_i(t) > 0$   $e_i(t)$  can be used to calculate the area of horizontal indentation into the prim  $A_{ip}(t)$  at every  $h_i(t)$  (17). The wear volume of both prisms  $\Delta V_p(t)$  can be calculated adding cylinder segments (18).

$$e_i(t) = r_i(t) - r_{ip}(t) \quad (16)$$

$$A_{ip}(t) = \{r_i(t)\}^2 * \arccos \left\{ 1 - \frac{e_i(t)}{r_i(t)} \right\} - \{r_i(t) - e_i(t)\} * \sqrt{2 * r_i(t) * e_i(t) - \{e_i(t)\}^2} \quad (17)$$

$$\Delta V_p(t) = 2 * \sum_i h_i(t) * A_{ip}(t) \quad (18)$$

### 3.2 3D-Plot

Besides the calculation of the wear volume, the profile information can be used to obtain a three-dimensional plot if a sufficient number of profiles per revolution is recorded. Therefore, the measured information of the profiles can be transferred into coordinates. Analog to Formula (10), the radial coordinates  $r_i(p)$  can be calculated. In addition, the vertical coordinates starting from the tip of the ball  $Z_i(p)$  can be calculated according to (19). With the rotational frequency of the specimen  $f_{spec}$  and the data acquisition rate  $f_{data}$  the circumferential coordinate  $\alpha(p)$  can be calculated (20). This circumferential coordinate can either be directly used for plotting or transferred in combination with the radial coordinates  $r_i(p)$  into X- and Y-coordinates. Afterwards the single data points can be triangulated to plot a surface mesh.

$$Z_i(p) = \frac{\sqrt{3}}{2} * [H_{i=0} - H_i] \quad (19)$$

$$\alpha(p) = p * 2 * \pi * \frac{f_{spec}}{f_{data}} \quad (20)$$

## 4 Results and Discussion

To get a better understanding of the evaluated wear data, two profiles at different times measured by the LPS are shown in Fig. 6. A freely rotating ball of AlMg3 was used so that no ball wear can occur. The data is plotted in the orientation of the LPS system. The initially calibrated rotational axis as well as the adjusted theoretical surface of the prim is

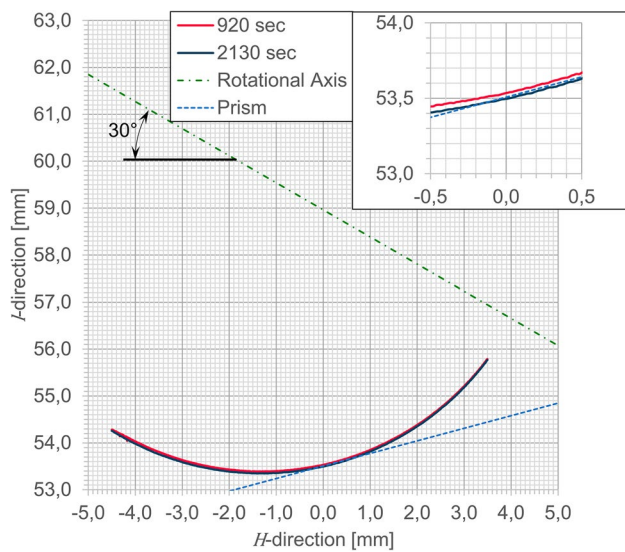


**Fig. 6** Profile data from the LPS of an AlMg3 ball (no wear) at different times and calibrated rotational axis

plotted. The rotational axis is tilted by  $30^\circ$  due to the  $30^\circ$  tilt angle of the LPS and the surface of the prism by  $45^\circ$  to the rotational axis. The two plotted data sets were deliberately chosen since they represent profiles with an approximately maximal observed deviation. This deviation—better visible in the scale up in the top right corner—can be explained by a small radial runout of the sample and the sample holder. Considering an ideally constant rotational speed of the ball being an integer multiple of the data acquisition rate the radial runout should not strongly influence the evaluation since the profile is always measured at the same position. This would lead to a constant offset of true to calculated wear volume. Since in the current setup of the VPS the rotational speed of the ball slightly differs from its target value, the profile is measured in slightly different positions. This leads to a scatter of the evaluated volume of the ball around a certain value with a certain amplitude. There are some possible measures to solve this issue. One possibility could be to reduce the diameter of the ball. This would not completely eliminate the scatter but strongly reduce it since the horizontal radii of the ball  $r_i(t)$  contribute in square to the volume of the ball and prism (refer Formula (11), (17) and (18)). From Formula (11) another possibility to reduce scattering can be derived. Reducing the recorded width ( $H$ -direction) in total leads to less  $h_i$  and therefore to a smaller  $V_k$  as well as a smaller scatter around it. However, this possibility is limited since the recorded width needs to be sufficiently high to record the complete area of wear. Another option is to improve the accuracy of the rotational speed of the ball so that it is a precise integer multiple of the data acquisition rate. This can be for example achieved by installing an encoded stepper motor as drive for the VPS6. A setup

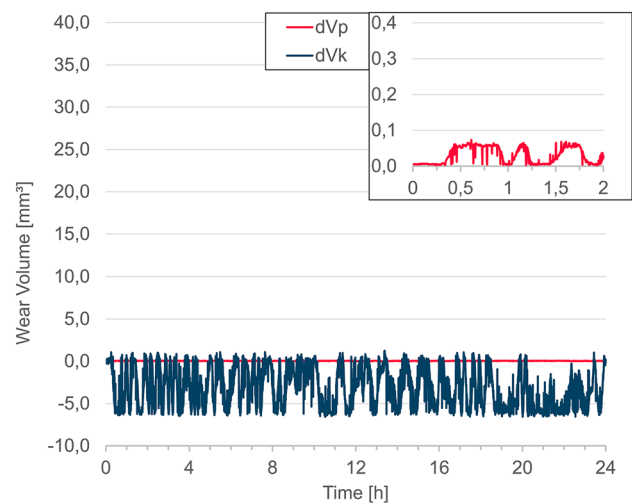


**Fig. 7** Evaluated theoretical 'wear volume' of a AlMg3 ball with no counter partner, data obtained with LPS and displacement transducer

like this would also allow to use the encoder of the stepper motor as a triggering device to trigger the data acquisition at a certain rotational position. Furthermore, controlled variation of rotational speeds during the test period can easily be achieved with this modification. A third simpler option is to install a triggering device at the test site which then triggers the data acquisition at a certain position of the ball.

In Fig. 7 the evaluated data from the first tested set can be found. As previously described, an AlMg3 ball was measured for 24 h without being in contact with a prism. The measurements deliver plausible results. As described in the previous paragraph slightly varying rotational speed in combination with the radial runout of the ball, leads to a scatter of the evaluated wear volume of the ball around a certain value with a certain amplitude. In this case approximately  $-2.5 \text{ mm}^3$  for both values. However, no increasing or decreasing trend can be found. The offset of the average value from zero can be explained by a radial runout. If for example the initial profile from which  $V_k(t = 0)$  is calculated is not the average case but one of the extreme cases, the average value of  $\Delta V_k(t)$  will be shifted by half the amplitude of the scattering (refer Formula (12)). These observations provide the general ability to measure the ball with the LPS system in-situ. Nevertheless, compared to sliding combinations with a rather small wear volume of the ball like for example in the range of  $2 \text{ mm}^3$  over 100 h [15] the signal to noise ratio in the current setup is too high to produce accurate results.

Looking at the calculated wear volume of the prism, a slight offset of approximately  $0.025 \text{ mm}^3$  of the mean value can be found as well as a certain scatter around this value. Similar to the wear volume of the ball, the scatter can be explained by the radial runout of the ball. As described in



the previous chapter for the calculation of the wear volume of the prism the shape of the worn ball is considered by determining the horizontal indentation into the prism  $e_i(t)$ . To be able to do this, the shape of the ball and therefore the incremental horizontal radii of the ball  $r_i(t)$  need to be considered (Formula (16)). Therefore, the radial runout of the ball also causes a scatter of the wear volume of the prism. Furthermore, the radial runout causes small imperfections during the determination of  $T$ . This again explains the small offset value of the wear volume of the prism. This however, leads to small offset of  $r_{ip}(t)$  causing an offset of  $e_i(t)$  and therefore the apparent wear volume of the prism (refer Formula (15) and (16)).

Figure 8 shows results from the second combination for validation (Table 1). With this combination, only the prism experiences wear. As in the previous tests, the same scatter of the wear volume of the ball as well as no significant increase over the test duration can be observed. In contrast to the previous case, the measurement was started more or less at the other extreme of the radial runout leading the average wear volume to be in the negative area. This however could be easily corrected by introducing an offset value shifting the average value towards the zero line. Looking at the wear volume of the prism calculated with the LPS data, a constantly increasing wear volume can be found. Comparing it to the data calculated only from the displacement transducer assuming that only the prism is worn, a similar curve propagation can be found. The wear volume calculated with the LPS data however is shifted to slightly higher values. This can be explained by small inaccuracies during adjustment of the initial position of the prism and the resulting value for  $T$ . It also explains why the values derived with the LPS data do not start at zero wear volume. Furthermore, the

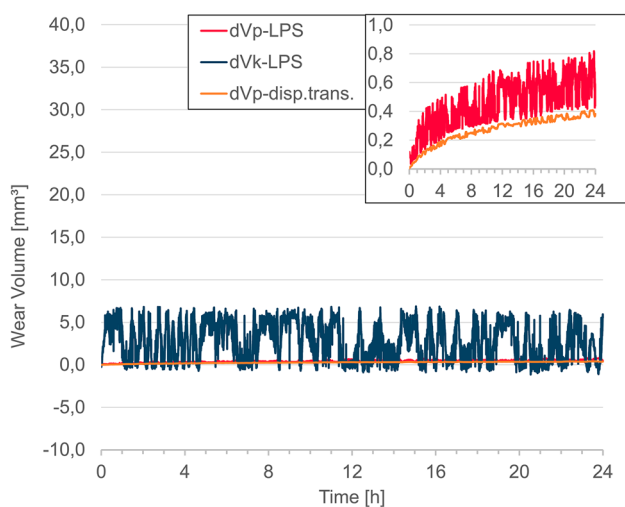


**Fig. 8** Evaluated wear volume of an AlMg3 ball against PETG/PTFE prism (case: only prism is worn), data obtained with LPS and displacement transducer

data obtained with the LPS system considers the true profile with which the prism is worn, rather than an idealized ball geometry during the evaluation of the indentation depth only. In addition, the thermal expansion caused by the frictional heat is now measured differently. During the test the ball and the prism will heat up to different extent due to the different contact ratio, volume and in case of different materials heat conductivity and heat capacity. When using only the data of the displacement transducer the thermal expansion of both partners will be consolidated as one and evaluated with the according calculation for the wear scenario. In contrast to that, the use of the LPS system leads to a separation of the thermal expansion of ball and prism, since the shape of the ball is directly measured. Yet another difference is that with the LPS system the elastic deformation of the ball directly during contact is not measured and therefore not included in the wear volume.

The results of the third case—PA66 ball sliding in 100Cr6 prism, no prism wear is expected—are shown in Fig. 9. As expected, the wear volume of the prism evaluated from the LPS data is more or less constant in the range of  $0.2 \text{ mm}^3$  very close to the zero line. On the other hand, the wear volume of the ball evaluated from the LPS is constantly increasing. Comparing it to the data calculated only from the displacement transducer assuming that only the ball wears, a similar curve propagation can be found. Similar to the previous results, the reason for the small deviation in between them lies in the fact that the LPS system measures the actual geometry. In contrast to that, the data calculated only from the displacement transducer calculates with an idealized spherical geometry. Despite these small differences, the measurement with the LPS system delivers plausible results.

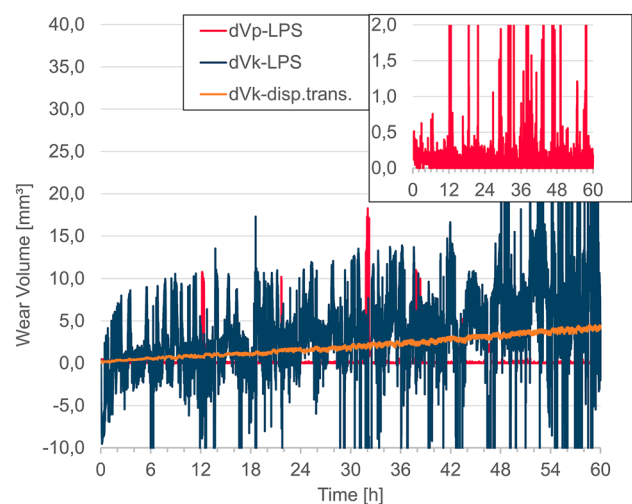


**Fig. 9** Evaluated wear volume of a PA66 ball against 100Cr6 prism (no wear of prism expected), data obtained with LPS and displacement transducer

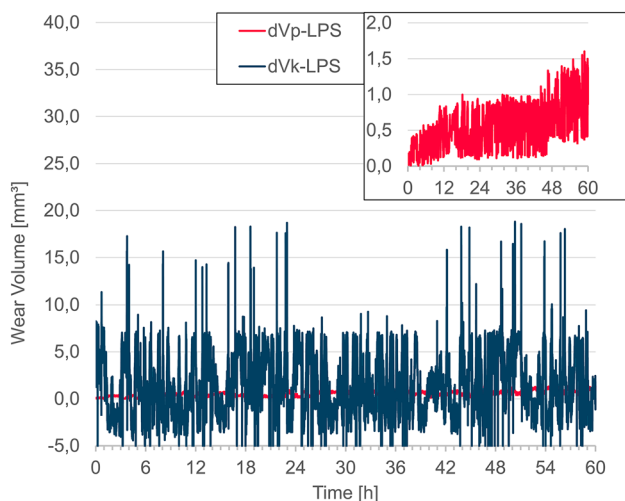
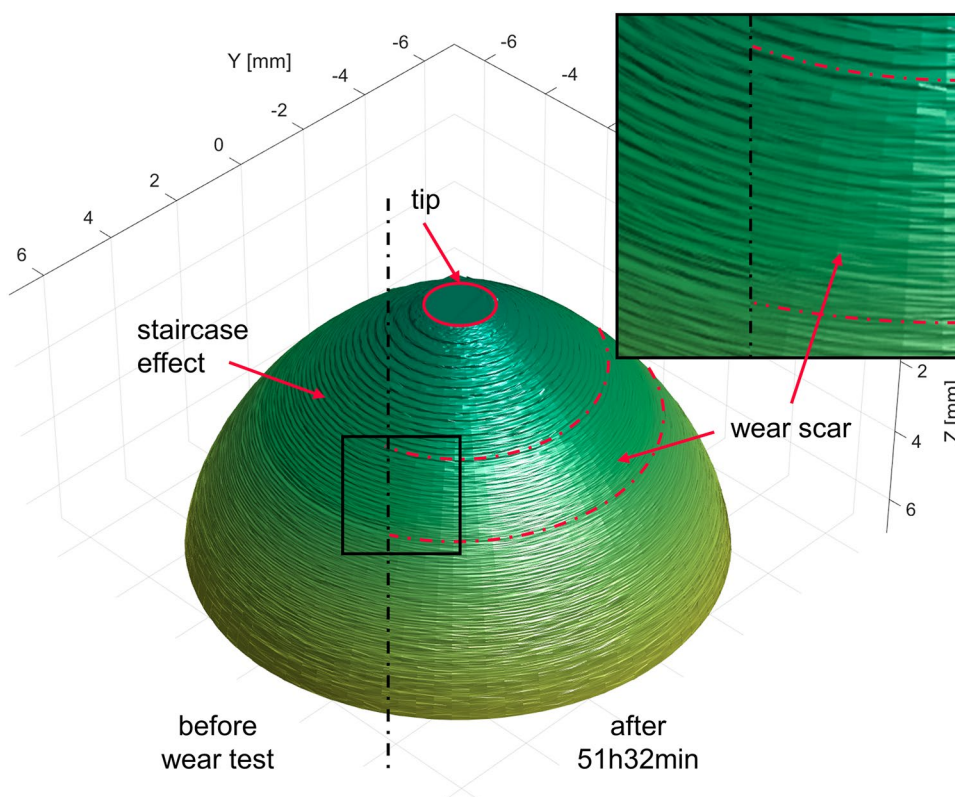


**Fig. 10** Evaluated wear volume of a PETG/PTFE ball against PLA prism, data obtained with LPS and displacement transducer

In Fig. 10, the result from the fourth material combination—PETG/PTFE ball sliding against a PLA prism—is shown. As we can see from the data, the wear occurs on the prism rather than on the ball. Overall a wear volume of round about 1 mm<sup>3</sup> over 60 h was observed at the prism.

Figure 11 shows 3D-images that were measured in-situ at different times of the previously described test. Each image is sampled from 100 profiles obtained during one revolution

**Fig. 11** 3D-images of a ball from PETG/PTFE running against PLA, 100 profiles per revolution



of the ball. Depending on the data acquisition frequency and the rotational speed—in this case 100 Hz and 1 Hz resulting in an angular resolution of 3.6°—relatively precise three-dimensional representations of the rotating specimen can be done. The use of similar LPS systems with data acquisition frequencies of up to 2000 Hz would allow to significantly increase rotational speed while still increasing angular resolution. Due to the orientation of the laser, the very tip of the ball cannot be properly measured and therefore is cut off. The images give a very detailed visual information of the evolving surface throughout the complete measurement as for example, roughening or smoothening effects. In a further step such three-dimensional representations can also be used to more accurately calculate the wear volume. However, this would drastically increase the amount of stored raw-data.

The stair case effect (0.1 mm height) of the printed specimen is clearly visible. Due to the layer-wise build-up of the specimen during printing, with increasing curvature towards the tip of the ball the staircase effect becomes more pronounced. Comparing the section before and during the wear test, we can see that a small area where the surface structure is slightly changed and the staircase effect is not visible anymore. This only very slight wear scar is in accordance with the previous results. During this test the ball shows no significant wear while the prism experiences most of the wear.

In contrast to the previous combination the fifth combination—POM ball against POM prism—shows wear on both partners. It is a good example why the presented new

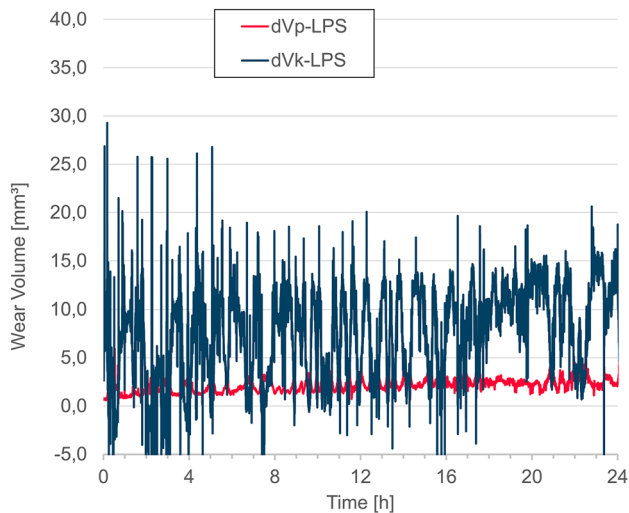
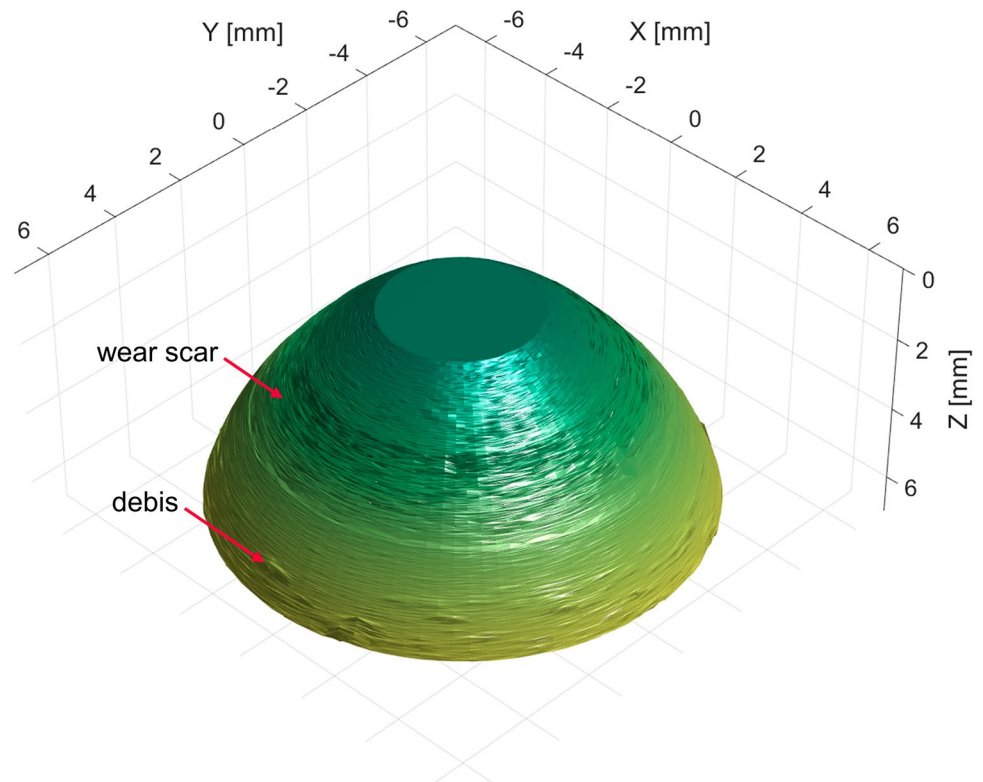


**Fig. 12** Evaluated wear volume of a POM ball against POM prism, data obtained with LPS and displacement transducer

measuring technique can be useful. The results are plotted in Fig. 12. While it's very clear that the wear volume of the prism constantly increases up to a value of approximately  $2.5 \text{ mm}^3$  after 24 h, the wear volume of the ball has a rather strong scatter. However, an increasing tendency for the wear volume can be observed. Looking at the 3D-image of the POM ball after 6h37min (Fig. 13) we can clearly see the

**Fig. 13** 3D-image of a ball from POM running against POM after 06:37, 100 profiles per revolution



wear scar on the ball. Furthermore, debris starting to accumulate on the ball can be found.

Despite the successfully proven concept, there are some challenges. The sixth combination—ASA ball against ASA Prism—is a good example. Figure 14 gives 3D-representations of the ASA ball before and during the wear test. The accumulation of debris around the wear scar is clearly visible. The ASA ball was removed from the test stand after completing the test. Even though some of the debris fell off during removal from the test stand, the photograph clearly shows the rings of debris. Comparing the profile before and during wear test at the marked position—refer Fig. 15—the accumulation of debris can be even seen better. Especially, in the magnification a clear border between the ball surface and the accumulated debris is clearly visible. Despite being able to generate 3D-images of the ball, in case of significant accumulations of debris around the wear mark on the ball, the calculation of the wear volume become rather challenging. The debris leads to an artificial increase in volume of the ball adulterating the wear volume of the ball and therefore also of the prism and the whole tribological system.

The same issue might occur if combinations are tested with certain opaque external lubricants, like PTFE or graphite. A first approach for a solution to this problem could be introducing a fit curve. The data points above and below the wear scar that are not adulterated by the debris can be used to create a ball fit. At every point where the radius measured by the LPS system is greater than its corresponding

**Fig. 14** 3D-image of a ball from ASA running against ASA after 23h19min, 100 profiles per revolution. Photograph shows the worn ball with remaining parts of the debris ring after disassembly from the test stand

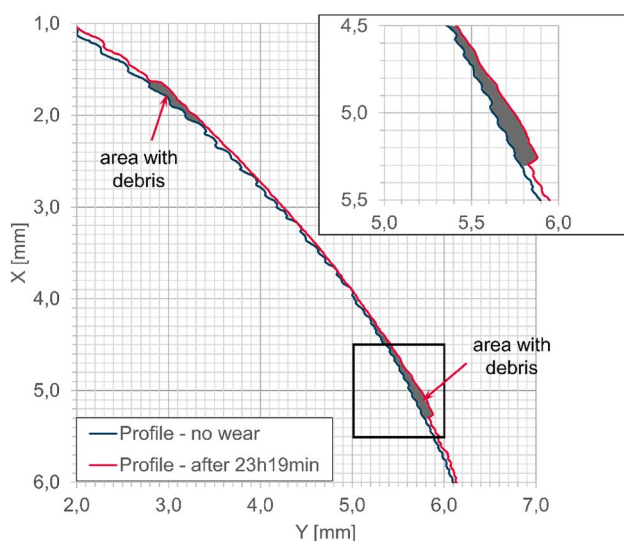
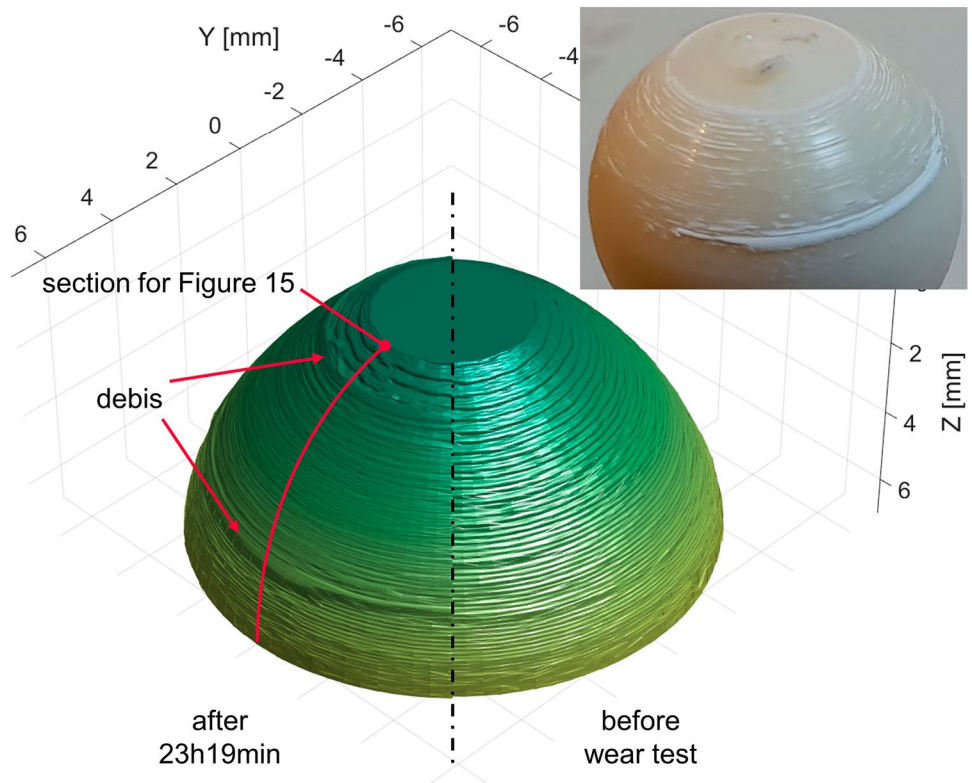


**Fig. 15** Profile data from the 3D-image of an ASA ball running against an ASA prism before wear test and after 23h19min showing the accumulation of debris

fitted value, it is replaced by the fitted value. This allows to subtract most of the accumulating debris. Nevertheless, the true profile of the ball cannot be measured resulting in some remaining inaccuracies.

Another challenge that arises is with wet lubricated combinations. Due to the opening in the prism required for profile measurement the lubricant will escape the system depending on its viscosity. Therefore, the system conditions will change over time which is unpreferable.

## 5 Conclusion

The results have proven the concept of in-situ differentiation of two simultaneously wearing counterparts, if at least one partner has an accessible area of the wear mark. However, for the described setup with a ball-on-prism tribometer there are challenges still to overcome. So far, in case of wear of the ball the technique does only deliver useful results for tribological combinations with rather large wear. The main reasons for this are the radial runout of the ball as well as the slightly varying rotational speed of the ball. However, both of these issues can be overcome by improving the VPS6 or adapting the measuring technique to another more precise tribological test stand.

The transferability of this method to other test stands is another great opportunity of the presented measuring technique. The classical pin-on-disc tribometer might be a very promising example. Similar to CN101504357A [17], the wear mark of the disc can be measured with the same LPS

system, the indentation depth can be measured at the pin using displacement transducers.

Considering all the aspects, the described method offers new possibilities for evaluation of the wear behavior, especially for simultaneously wearing counterparts. Nevertheless, like all other tribological test method this is not an all-in-one solution. Especially testing in media as well as excessive amounts of debris that can accumulate in the measuring field of the LPS are major challenges. In addition, there is still room for improvement especially in software programming. For example, implementing a trigger signal for the profile measurement would allow to measure the ball always at the same spot.

**Supplementary Information** The online version contains supplementary material available at <https://doi.org/10.1007/s11249-023-01759-8>.

**Acknowledgements** We would like to thank the Technische Hochschule Lübeck, especially the Department of Mechanical Engineering and Business Administration for the financial support of this research project.

**Author Contributions** FH: Conceptualization, Investigation, Software, Methodology, Validation, Formal analysis, Writing—Original Draft, Visualization; BS: Investigation, Writing—Review & Editing; MS: Software RK: Software, Writing—Review & Editing, Supervision; RA: Supervision; OJ: Writing—Review & Editing, Supervision.

**Funding** Open Access funding enabled and organized by Projekt DEAL. This research was funded by Technische Hochschule Lübeck Department of Mechanical Engineering and Business Administration.

**Data Availability** The research data will be made available on request.

## Declarations

**Conflict of interest** The authors have no relevant financial or non-financial interests to disclose.

**Open Access** This article is licensed under a Creative Commons Attribution 4.0 International License, which permits use, sharing, adaptation, distribution and reproduction in any medium or format, as long as you give appropriate credit to the original author(s) and the source, provide a link to the Creative Commons licence, and indicate if changes were made. The images or other third party material in this article are included in the article's Creative Commons licence, unless indicated otherwise in a credit line to the material. If material is not included in the article's Creative Commons licence and your intended use is not permitted by statutory regulation or exceeds the permitted use, you will need to obtain permission directly from the copyright holder. To view a copy of this licence, visit <http://creativecommons.org/licenses/by/4.0/>.

## References

- Santner, E., Czichos, H.: Tribology of polymers. *Tribol. Int.* **22**(2), 103–109 (1989). [https://doi.org/10.1016/0301-679X\(89\)90170-9](https://doi.org/10.1016/0301-679X(89)90170-9)
- Rymuza, Z.: Tribology of polymers. *Archives Civil Mech. Eng.* **7**(4), 177–184 (2007). [https://doi.org/10.1016/S1644-9665\(12\)60235-0](https://doi.org/10.1016/S1644-9665(12)60235-0)
- Myshkin, N.K., Pesetskii, S.S., Grigoriev, A.Y.: Polymer tribology: current state and applications. *Tribol. Ind.* **37**(3), 284 (2015)
- Hu, C., Qi, H., Song, J., Zhao, G., Yu, J., Zhang, Y., He, H., Lai, J.: Exploration on the tribological mechanisms of polyimide with different molecular structures in different temperatures. *Appl. Surf. Sci.* **560**, 150051 (2021). <https://doi.org/10.1016/j.apsusc.2021.150051>
- Theiler, G., Gradt, T.: Influence of counterface and environment on the tribological behaviour of polymer materials. *Polym. Test.* **93**, 106912 (2021). <https://doi.org/10.1016/j.polymertesting.2020.106912>
- Walczak, M., Caban, J.: Tribological characteristics of polymer materials used for slide bearings. *Open Eng.* **11**(1), 624–629 (2021). <https://doi.org/10.1515/eng-2021-0062>
- Pradeepkumar, C., Karthikeyan, S., Rajini, N.: A short review on the effect of transfer layer on tribological study of composite materials. *Mater. Today: Proceed.* **50**, 2073–2077 (2022). <https://doi.org/10.1016/j.matpr.2021.09.416>
- Hanon, M.M., Ghaly, A., Zsidai, L., Klebert, S.: Tribological characteristics of digital light processing (DLP) 3D printed graphene/resin composite: influence of graphene presence and process settings. *Mater. Design* **218**, 110718 (2022). <https://doi.org/10.1016/j.matdes.2022.110718>
- Friedrich, K.: Polymer composites for tribological applications. *Adv. Ind. Eng. Polym. Res.* **1**(1), 3–39 (2018). <https://doi.org/10.1016/j.aiepr.2018.05.001>
- Ballesteros, L.M., Zuluaga, E., Cuervo, P., Rudas, J.S., Toro, A.: Tribological behavior of polymeric 3D-printed surfaces with deterministic patterns inspired in snake skin morphology. *Surf. Topogr.: Metrol. Prop.* **9**(1), 014002 (2021). <https://doi.org/10.1088/2051-672X/abe211>
- Prabhu, R., Devaraju, A.: Recent review of tribology, rheology of biodegradable and FDM compatible polymers. *Mater. Today Proceed.* **39**, 781–788 (2021). <https://doi.org/10.1016/j.matpr.2020.09.509>
- Panin, S.V., Buslovich, D.G., Kornienko, L.A., Alexenko, V.O., Dontsov, Y.V., Shil'ko, S. V.: Structure, as well as the tribological and mechanical properties, of extrudable polymer-polymeric UHMWPE composites for 3D printing. *J. Frict. Wear* **40**, 107–115 (2019)
- Panin, S.V., Buslovich, D.G., Kornienko, L.A., Aleksenko, V.O., Dontsov, Y.V., Ovechkin, B.B., Shil'ko, S. V.: Comparative analysis of tribological and mechanical properties of extrudable polymer-polymer UHMWPE composites fabricated by 3D printing and hot-pressing methods. *J. Frict. Wear* **41**, 228–235 (2020). <https://doi.org/10.3103/S1068366620030125>
- Schädel, B., Rüdiger, G., Jacobs, O., Kowtun, A., Beneke, T.: Verschleißverhalten von Kunststoff-Kunststoff-Paarungen. *Tribol. Schmierungstech.* **59**(3), 29–34 (2012). <https://doi.org/10.3103/S1068366619020090>
- Harden, F., Schädel, B., Kral, R., Siebert, L., Adelung, R., Jacobs, O.: Wear behavior of additive manufactured polymer-polymer sliding combinations. *Tribol. Schmierungstech.* **68**(2), 15 (2021). <https://doi.org/10.24053/TuS-2021-0010>
- Jacobs, O., Jaskulka, R., Yan, C., Wu, W.: On the effect of counterface material and aqueous environment on the sliding wear of various PEEK compounds. *Tribol. Lett.* **18**, 359–372 (2005). <https://doi.org/10.1007/s11249-004-2766-3>
- 刁东风, 张立章, 范雪. (2009). Friction wear testing machine for on-line measurement (CN101504357A). State Intellectual Property Office (China).
- 武通海, 彭业萍, 张小刚, 张乐. (2012). Abrasion in-situ measuring device based on digital image processing and method (CN102607977B). State Intellectual Property Office (China).

19. Vishal Khosla, Nick Doe, Ming Chan, Jun Xiao, Gautam Char. (2017). Method for in-line testing and surface analysis of test material with participation of raman spectroscopy (US10258239B2). United States Patent and Trademark Office (US).
20. Vishal Khosla, Nick Doe, Jun Xiao, Ming Chan, Gautam Char. (2016). Apparatus for in-line testing and surface analysis on a

mechanical property tester (US10024776B2). United States Patent and Trademark Office (US).

**Publisher's Note** Springer Nature remains neutral with regard to jurisdictional claims in published maps and institutional affiliations.